

Neural Networks for Implicit Representations of 3D Scenes

Luiz Schirmer; Guilherme Schardong; Vinícius da Silva and Hélio Lopes

Pontifícia Universidade Católica do Rio de Janeiro - PUC-Rio

Tiago Novello; Daniel Yukimura; Thales Magalhaes; Hallison Paz and Luiz Velho

Instituto de Matemática Pura e Aplicada - IMPA

Abstract—This survey presents methods that use neural networks for implicit representations of 3D geometry — *neural implicit functions*. We explore the different aspects of neural implicit functions for shape modeling and synthesis. We aim to provide a theoretical analysis of 3D shape reconstruction using deep neural networks and introduce a discussion between researchers interested in this research field.

I. INTRODUCTION

Representing shapes as level sets of neural networks has recently been useful for different shape analysis and reconstruction tasks. Computer graphics and 3D computer vision presented multiple approaches to representing 3D geometry for rendering and reconstruction, providing trade-offs across fidelity, efficiency, and compression capabilities. This survey presents methods to model geometry and appearance with Neural Networks that provide extrinsic descriptions, including: i) Spatial Characteristic Functions; ii) Signed Distance Functions (SDFs); and iii) Volumetric Fields. We explore seminal works considering the state-of-the-art high-quality shape representation, interpolation, and completion from partial noisy 3D input data and also image collections. Considering these techniques, implicit data representation can be computed by implicit regularization, periodic activation functions, and loss functions among others explicitly defined over the neural level sets. We also present methods to enhance the performance of these deep neural networks, where it can be possible to be used in real-time applications.

II. TOPIC SURVEY

We start giving an overview of the main concepts involved in this topic followed by a classification of the state of the art and recent research work in this area.

A. Main Concepts

The main concepts related to Neural Implicit Representations correspond to the shape and appearance models as well as to the usage of neural networks in these descriptions.

1) *Neural Parametric Surfaces*: Explicit geometric representations describe a surface intrinsically, i.e., by a parametric function $g : U \subset \mathbb{R}^2 \rightarrow \mathbb{R}^3$. In that context, a surface can be represented by an atlas, where each chart is a local parameterization [1].

In order to model this kind of representation by a Neural Network, Groueix et al. [2] and Deprelle et al. [3] suggested modeling charts as Multi-layer perceptrons (MLPs) and

Williams et al. [4] focused on individual surface reconstructions. Some works have considered global surface parametrizations [5]–[7]. Global parametrizations produce consistent coverings, although they introduce high distortions [1]. However, parametric representations over implicit neural representations have some disadvantages: it isn't straightforward to produce perfectly overlapping charts.

2) *Neural Implicit Surfaces*: Implicit geometric representations describe a surface extrinsically, i.e., by a function of the ambient space $f : \mathbb{R}^3 \rightarrow \mathbb{R}$ that classifies the points of an embedded object. Differently from explicit geometric representations, such as vertex and triangle lists, implicit descriptions, such as *signed distance functions* (SDFs) may be used to represent geometry, where the object is the zero-level set of a function defined in the space. More formally, in the particular case of SDFs, let $f : \mathbb{R}^3 \rightarrow \mathbb{R}$ be a smooth function, f is a signed distance function from $f^{-1}(0)$ if it satisfies the *Eikonal equation* $\|\nabla f\| = 1$. The zero-level set $f^{-1}(0)$ of f is a *hypersurface* in \mathbb{R}^3 defined by all points $\mathbf{X} \subset \mathbb{R}^3$ satisfying $f(\mathbf{X}) = 0$. Such representation allows for simple collision tests, continuous (vs. discrete) representation, and differentiability.

B. Model Classification

Recent work in the area of Neural Implicit Representations of 3D Scenes can be classified according to the type of implicit description employed and also by the way it is implemented using a Neural Network.

In that context, we divide the methods in four categories:

- 1st Generation Models
- 2nd Generation Models
- 3rd Generation Models
- 4th Generation Models

It is noteworthy to point out that the evolution of the area followed the developments of these models in chronological order.

1) *1st Generation Models*: The First Generation Models correspond to *global* functions of the ambient space and employ as implicit model either the *characteristic function* or the *signed distance function*. They use a fully connected Multi Layer Perceptron (MLP) network architecture. The model is learned by fitting the input data to the model. The Loss function is based either on the $L1$ or $L2$ norm.

86 The seminal papers of this category appeared in 2019. They
 87 are: Occupancy Networks [8], LIF [9], Deep SDF [10], and
 88 Deep Level Sets [11].

89 2) *2nd Generation Models*: The Second Generation Models
 90 correspond to a set of *local* functions that combined together
 91 gives a representation of a function over the whole space.
 92 These models are based either on a shape algebra, such
 93 as in Constructive Solid Geometry (CSG), or Convolutional
 94 Operators.

95 The seminal papers of this category appeared in 2019 /
 96 2020. They are: LDIF (Genova et al, 2019), BSP-Net [12],
 97 CvxNet [13] and Convolutional Occupancy Networks [14].

98 3) *3rd Generation Models*: The Third Generation Models
 99 correspond to true signed distance functions (SDF) that are
 100 given by the *Eikonal* equation. The model exploits in the Loss
 101 function the condition that the gradient of the function has
 102 to be constant and with norm equal to one everywhere, i.e.,
 103 $\|\nabla f\| = 1$.

104 The seminal papers of this category appeared in 2020. They
 105 are: IGR [1] and SIREN [15].

106 4) *4th Generation Models*: The Fourth Generation Models
 107 correspond to continuous volumetric functions that encode
 108 *light fields*. They represent geometry as a density over space
 109 and also encode direction-dependent radiance information.

110 The seminal papers of this category appeared in 2020 /2021.
 111 They are: NeRF [16], MNSR [17], among others.

112 III. FIRST GENERATION MODELS

113 A. Occupancy Networks

114 Many of prior learning based 3D reconstruction approaches
 115 can only represent very coarse 3D geometry or are limited to
 116 a restricted domain. Occupancy networks implicitly represent
 117 the 3D surface as the continuous decision boundary of a deep
 118 neural network classifier. In contrast to previous approaches,
 119 that representation encodes a description of the 3D output at
 120 infinite resolution without excessive memory footprint.

121 The main idea is to reason occupancy not only at fixed
 122 discrete 3D locations (as in voxel representations) but at
 123 every possible 3D point $p \in \mathbb{R}^3$. This is done by defining
 124 an occupancy function $o : \mathbb{R}^3 \rightarrow \{0, 1\}$ that this network
 125 is equivalent to a neural network for binary classification,
 126 except that we are interested in the decision boundary which
 127 implicitly represents the object's surface. See Figure 1.

128 When using such a network for 3D reconstruction of an
 129 object based on observations of that object (e.g., image, point
 130 cloud, etc.), it must be conditioned on the input. Fortunately, a
 131 simple functional equivalence can be used for this: a function
 132 that takes an observation $x \in X$ as input and has a function
 133 from $p \in \mathbb{R}^3$ to \mathbb{R} as output can be equivalently described
 134 by a function that takes a pair $(p, x) \in \mathbb{R}^3 \times X$ as input
 135 and outputs a real number. The latter representation can be
 136 simply parameterized by a neural network f_θ that takes a pair
 137 (p, x) as input and outputs a real number which represents the
 138 probability of occupancy: $f_\theta : \mathbb{R}^3 \times X \rightarrow \{0, 1\}$ (2). This
 139 network is called the Occupancy Network.

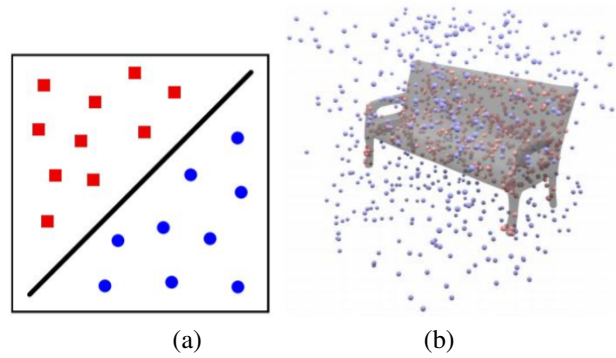


Fig. 1. Occupancy Network as decision Boundary (a) and Classification of Points in Space (bb).

140 B. Deep SDF

141 Differently from previous works, [10] proposed a continu-
 142 ous approach for learning 3D shapes. Instead of modelling the
 143 shapes explicitly, i.e. by triangle meshes, they proposed using
 144 an implicit representation with Signed Distance Functions. The
 145 target shape is the zero level-set of this function ($\forall x$ such that
 146 $F(x) = 0$, where $F(\cdot)$ is the signed distance function). See
 147 Figure 2.

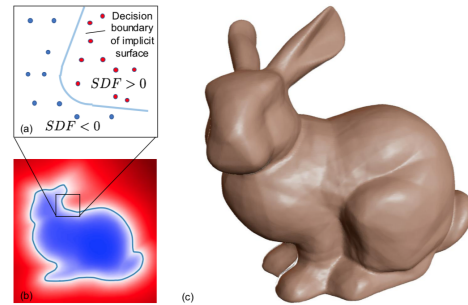


Fig. 2. Deep SDF Implicit Function.

148 This modelling choice enabled them to make use of the Uni-
 149 versal Approximation Theorem for multi-layer perceptrons.
 150 Thus, they proposed a MLP model to approximate the SDF
 151 representation of a target shape by using points sampled from
 152 the domain as input, and their SDF values as targets. A clear
 153 advantage of this approach is the ability to learn a continuous
 154 representation of the function, being limited only by the model
 155 capacity.

156 Another aspect of DeepSDF is the ability to learn not only a
 157 single shape, but a family shapes. By adding a latent vector as
 158 an encoder of the target shape, the model is able to map and
 159 learn a latent representation of the shape itself. Thus, one may
 160 change a latent code while maintaining the point sample as a
 161 sort of "index" to the desired shape. This also allows for shape
 162 interpolation by performing a linear interpolation between
 163 distinct latent vectors. See Figure 3. The authors propose an
 164 encoder-less approach to learn this latent representation, being
 165 the first work to do so in the graphics learning community, to
 166 the best of our knowledge.

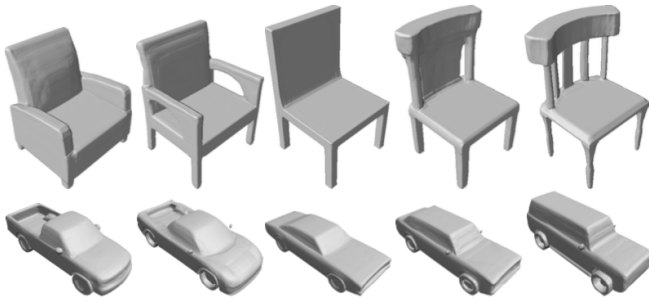


Fig. 3. Interpolation of Shape Families.

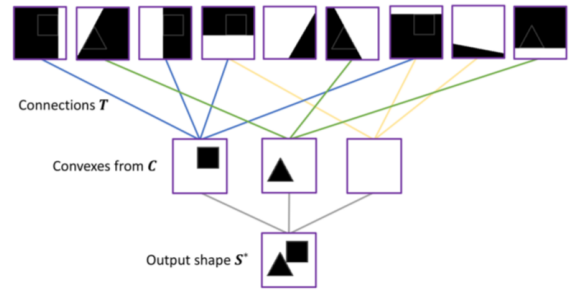


Fig. 4. Neural BSP Tree.

IV. SECOND GENERATION MODELS

A. BSP-Net / CvxNet

Let $\{m_i, g_i\}$ be a given *data-set*. m_i are elements in the *input set* \mathcal{X} (images, point clouds, or voxel grids). $g_i : \mathbb{R}^3 \rightarrow \mathbb{R}$ are implicit functions representing objects \mathcal{O}_i . Specifically, the object surface $\partial\mathcal{O}_i$ is $\{p | g_i(p) = 0\}$, its interior is $\{p | g_i(p) < 0\}$ and $\{p | g_i(p) > 0\}$ is the exterior. Suppose that $f(\cdot, m_i) = g_i(\cdot)$ for some unknown function $f : \mathbb{R}^3 \times \mathcal{X} \rightarrow \mathbb{R}$. The *deep implicit problem* is the task of constructing a function f_θ that approximates f . Once we find a “good” function f_θ , we estimate the object associated with an unknown input $m \in \mathcal{X}$ using $f_\theta(\cdot, m)$. This section presents two networks that solve this problem using *constructive solid geometry* (CSG): CvxNet [13] and BSP-Net [12].

In CSG, *boolean operators* (union, intersection, ...) are used to combine simpler objects to create complex ones. CSG *objects* can be represented by *trees*. The *leaves* correspond to primitives (half-space, cubes, balls, ...) and the *nodes* represent operations. CvxNet and BSP-Net are networks that encode simple CSG trees. The leaves (primitives) are half-spaces, an intermediate layer considers the intersections of the half-spaces to form convex shapes and, finally, the root of the tree is obtained through the union operator that groups the convexes into a single shape.

Given an input $m \in \mathcal{X}$, BSP-Net learns a (CSG) implicit function $f_\theta(\cdot, m) : \mathbb{R}^3 \rightarrow \mathbb{R}$. This network consists of three steps. First, an encoder receives the input m and returns a feature code that is the input of an MLP layer. This layer produces the parameters that define a fixed number of plane equations $ax + by + cz + d = 0$. These implicit functions are evaluated on n points (in homogeneous coordinates). The second step considers a binary matrix that forces a collection of half-planes to form a fixed number of convex polytopes. Finally, the last layer groups these convex parts producing the desired implicit function f_θ . Given a new input $m' \in \mathcal{X}$, observe that the zero-level set of $f_\theta(\cdot, m')$ is a surface with *sharp* details since it is the boundary of the union of convex polytopes. Note also that the considered binary matrix learns edges between the half-planes and the convex polytopes, therefore, BSP-Net “learns” the CSG tree. See Figure 4.

The CSG tree is fixed in the CvxNet. However, this network represents a finite family of smooth convex shapes.

Specifically, given an input $m \in \mathcal{X}$ an encoder estimates a feature vector λ representing a family of smooth convex shapes. A decoder takes λ and returns a collection of parameter tuples. Each tuple consists of a vector storing the half-space coefficients used to create the corresponding smooth convex. Combining the implicit functions related to these convex shapes gives rise to the desired implicit function f_θ .

Some examples can be seen in Figure 5.

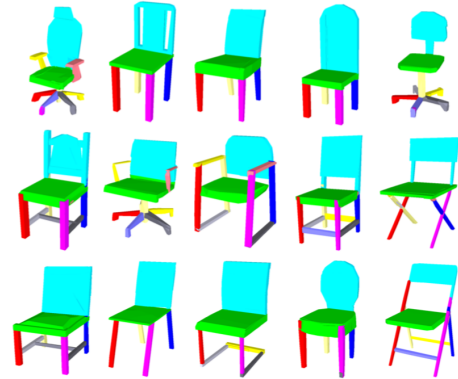


Fig. 5. Correspondence between Decomposition of Structurally Similar Models.

B. Convolution Occupancy Networks

Implicit approaches show exciting results; however, most of the works are limited to analyze simple geometries of single objects. The main related works do not scale to large scenes with higher quality and details. The main factor that may exploit the limitations of these methods is their simple fully-connected network architecture which does not allow for integrating local information in the observations or incorporating inductive biases such as translation equivariance. Peng et al. propose the Convolutional Occupancy Networks, which the author says is a more flexible representation for a detailed reconstruction of objects and 3D scenes.

The main idea is simple but clever: they combine convolutional encoders with implicit occupancy decoders. The method exploits convolutional operations to obtain translation equivariance and the local similarity of 3D structures. They query convolutional features at 3D locations using linear interpolation. In contrast with traditional occupancy networks,

235 this method depends on both input x and the 3D locations. The
 236 neural network first processes the input x to obtain a feature
 237 encoding for every point or voxel. They use a 3D CNN for
 238 voxelized inputs and a shallow PointNet with local pooling
 239 for 3D point clouds to construct planar and volumetric feature
 240 representations to encapsulate local neighborhoods.

241 The proposed representation can reconstruct geometry from
 242 noisy point clouds and low-resolution voxels. The method
 243 scale to large indoor scenes and generalizes from synthetic
 244 to real data when compared with Occupancy Networks as we
 245 can see in figure 6.

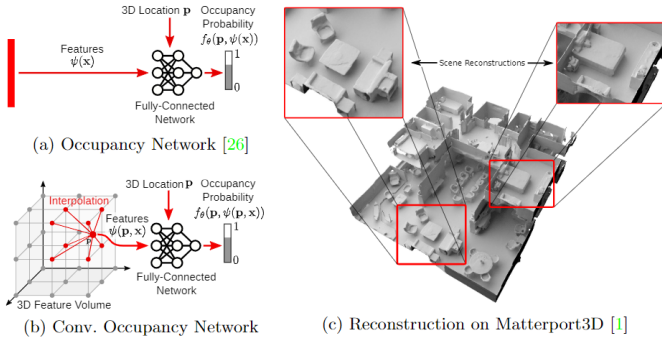


Fig. 6. Comparison between Convolutional Occupancy Networks and the traditional one from Peng et al. that shows a reconstruction of a two-floor building from a noisy point cloud on the Matterport3D dataset.

246 V. THIRD GENERATION MODELS

247 A. Siren

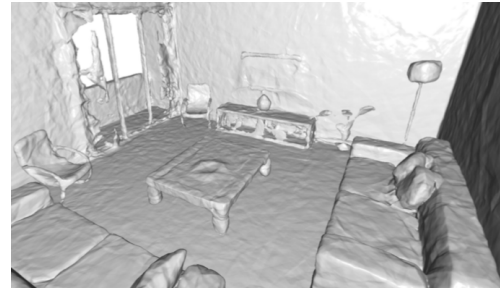
248 As we have seen in so far in this survey, implicitly defined,
 249 continuous signal representations by neural networks have
 250 emerged as a powerful paradigm, offering many possible ben-
 251 efits over conventional representations. However, the network
 252 architectures presented in the previous sections for such im-
 253 plicit neural representations are incapable of modeling signals
 254 with fine detail, and fail to represent a signal’s spatial and
 255 temporal derivatives, despite the fact that these are essential
 256 to many physical signals defined implicitly as the solution to
 257 partial differential equations.

258 Sitzmann et al. [15] proposes to leverage periodic activation
 259 functions for implicit neural representations and demonstrate
 260 that these networks are ideally suited for representing complex
 261 natural signals and their derivatives. SIRENs can be used for
 262 high quality reconstruction of objects and 3D scenes as we
 263 can see in Figures 7, 8 and 9.

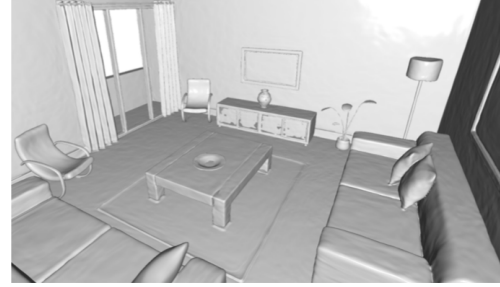
264 *SIREN* [15] — *sinusoidal representation networks* — can
 265 be used in order to approximate a sampled implicit function
 266 $f : \mathbb{R}^3 \rightarrow \mathbb{R}$. SIREN has important properties that are suitable
 267 for reconstructing signal, where it has a simple architecture
 268 and uses the sine as a periodic activation:

$$f_\theta(p) = W_n \circ f_{n-1} \circ f_{n-2} \circ \dots \circ f_0(p) + b_n, \quad (1)$$

$$f_i(p_i) = \sin(W_i \cdot p_i + b_i), \quad (2)$$



(ReLU)



(SIREN)

Fig. 7. A SIREN network used for shape representation. The signed distance function is fitted from a point cloud. Compared to a ReLU implicit representation it higher quality for complex 3D scenes.

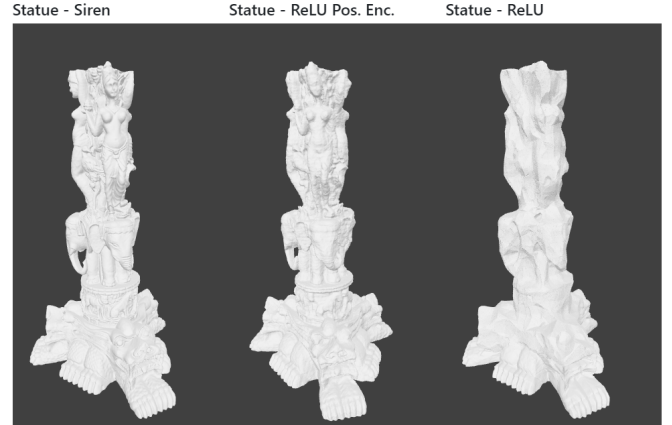


Fig. 8. The SIREN network recovers an SDF from a pointcloud and surface normals by solving the Eikonal equation, a first-order boundary value problem. SIREN can recover a 3D shape given only its pointcloud and surface normals.

270 where the function $f_i : \mathbb{R}^{N_i} \rightarrow \mathbb{R}^{N_{i+1}}$ is the i th layer of the
 271 network. This map is obtained by applying the sine to each
 272 coordinate of the affine map given by the linear transformation
 273 $W_i : \mathbb{R}^{N_i} \rightarrow \mathbb{R}^{N_{i+1}}$ translated by $b_i \in \mathbb{R}^{N_{i+1}}$. The linear
 274 operators W_i can be represented as matrices and b_i as vectors,
 275 therefore, the union of their coefficients correspond to the
 276 coefficients θ of the SIREN function f_θ . In other words, f_θ is
 277 parameterized by θ .

278 1) *SIREN is smooth*: The SIREN function f_θ is smooth
 279 since its partial derivatives (of all orders) exist and are contin-
 280 uous. Indeed, each function f_i has all the partial derivatives
 281 because, by definition, it is an affine map with the sine
 282 applied to each coordinate. Then, the chain rule implies the

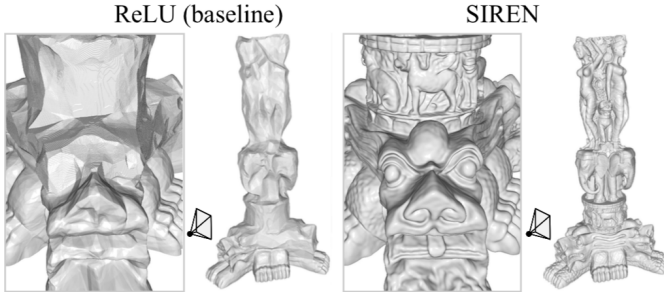


Fig. 9. SIREN significantly improves fine details of objects.

smoothness of f_θ .

We can derive the gradient of f_θ using the chain rule:

$$\begin{aligned} \nabla f_\theta(p) &= \mathbf{J}(W_n \circ f_{n-1} \circ \dots \circ f_0(p)) + \mathbf{J}(b_n) \\ &= \mathbf{J}W_n(p_n) \circ \mathbf{J}f_{n-1}(p_{n-1}) \circ \dots \circ \mathbf{J}f_1(p_1) \circ \mathbf{J}f_0(p), \end{aligned}$$

where \mathbf{J} is the *Jacobian* operator and $p_i = f_{i-1} \circ \dots \circ f_0(p)$. Using the facts that $\mathbf{J}(b_n) = 0$ because b_n is constant, and that $\mathbf{J}(W_n)(q) = W_n$ because W_n is linear, we obtain:

$$\nabla f_\theta(p) = W_n \circ \mathbf{J}f_{n-1}(p_{n-1}) \circ \dots \circ \mathbf{J}f_1(p_1) \circ \mathbf{J}f_0(p),$$

where $\mathbf{J}f_i(p_i) = W_i \odot \cos[a_i | \dots | a_i]$. The operator \odot is the *Hadamard* product, and the matrix $[a_i | \dots | a_i]$ has N_i copies of the vector $a_i = W_i(p_i) + b_i \in \mathbb{R}^{N_i+1}$.

2) *SIREN SDF functional*: Let $\{p_i, N_i\}$ be a sample of points $\{p_i\}$ and their normals $\{N_i\}$ on a compact surface S embedded in the cube $\mathcal{Q} = [-1, 1]^3$, Sitzmann et al. [15] proposed to fit the zero-level set of a SIREN function f_θ to $\{p_i, N_i\}$ forcing f_θ to be a *signed distance function* (SDF). More precisely, they required $f_\theta(p_i) = 0$, $\nabla f_\theta(p_i) = N_i$, and $|\nabla f_\theta(p)| = 1$. The first two equations force the SIREN function f_θ to be zero at the sampled points $\{p_i\}$ and the gradient of f_θ to be aligned to the sampled normals $\{N_i\}$. The equation $|\nabla f_\theta(p)| = 1$ is the *Eikonal* constraint, this is the differential equation for which the solution is a signed distance function. In particular, when we require $f_\theta(p_i) = 0$, it turns out that such restrictions are a sample of the initial condition that we would like to be $f_\theta(p) = 0$ for every $p \in S$.

The *loss function* used in the training [15] of the SIREN function f_θ is very similar to Equation 3:

$$\int_{\mathcal{Q}} |1 - \|\nabla f_\theta(p)\|| dp + \int_S |f_\theta| + (1 - \nabla f_\theta \cdot N) dS + \int_{\mathcal{Q}/S} e^{\alpha |f_\theta(p)|} dp \quad (3)$$

The term $e^{\alpha |f_\theta(p)|}$ in Equation 3, with $\alpha < -1$, penalizes the points outside the surface S . The function f_θ is supervised using the sample of points $\{p_i, N_i\}$. To train the coefficients θ , the authors used a *minibatch* containing an equal number of points on and off the surface S . The *on-surface* points were uniformly sampled on the point cloud $\{p_i, N_i\}$, and the *off-surface* points were uniformly sampled on the cube \mathcal{Q} .

B. IGR - Implicit Geometric Regularization

Implicit representations can be computed using implicit shape representations or loss functions explicitly defined over the neural level sets [18], [19]. The authors of IGR offer a new paradigm for computing high fidelity implicit neural representations directly from raw data in this technique. They observe that a relatively simple loss function, similar to the loss function in SIREN, encourages the neural network to vanish on the input point cloud and to have a unit norm gradient. The authors propose a technique called implicit geometric regularization (IGR) [1]. This method drives the optimization methods to reach a plausible interpretation for the learning and favors smooth and natural zero-level set surfaces. An example of how this method perform shape analysis can be seen in Figure 10.

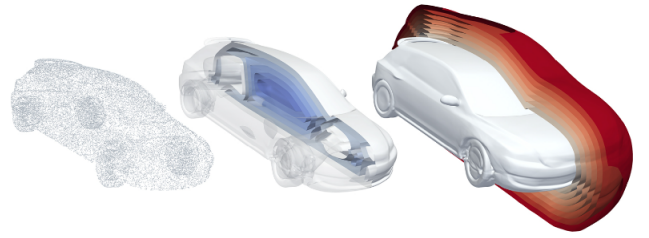


Fig. 10. The level sets of an MLP trained with the IGR method on an input point cloud; positive level sets are in red; negative are in blue; the zero level set, representing the approximated surface, is in white.

VI. FOURTH GENERATION MODELS

A. NeRF

Neural Radiance Fields (NeRF) [16] generates a novel view from a set of surrounding images and camera poses by representing a scene as a volumetric object and parameterizing it using a neural network. For each 3D point in space and observation direction, the neural network outputs an RGB color and a volume density value. Notice that volume rendering is naturally differentiable and, by using this approach, they were able to optimize the density values as a function of the location and predict the RGB color as a function of both location and viewing direction.

Ray marching through a volume can be a highly costly procedure. To address this issue, the authors propose to optimize two networks simultaneously, so that the output densities of a coarse version could be used to produce more informed sampling of points along the rays for a more refined version. This way, it's possible to do a hierarchical sampling of the scene. This technique demonstrated the capability of representing reflections and specularities when the observation view direction changes, as well as estimating depth information for consistent occlusion tests. See Figure 11.

B. Multiview neural surface reconstruction by disentangling geometry and appearance

In this work, the authors [17] introduce a neural network architecture that simultaneously learns the unknown geometry,

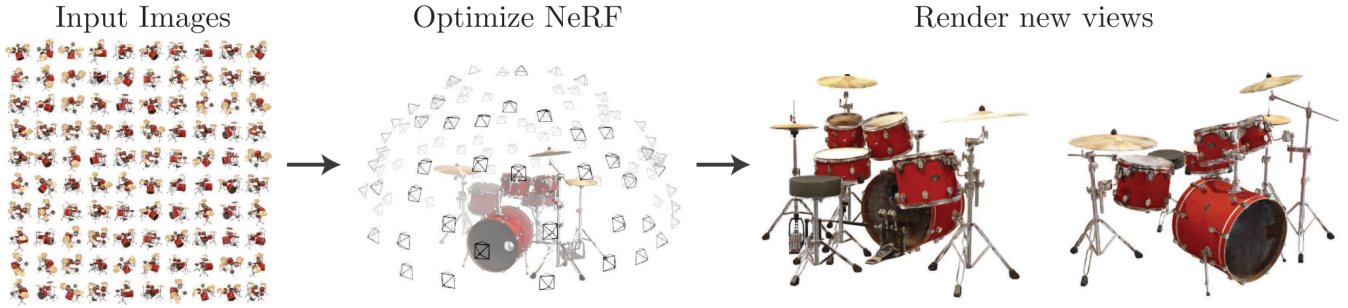


Fig. 11. NeRF

351 camera parameters, and a neural renderer [20] that approxi- 366
 352 mates the light reflected from a surface towards the camera. 367
 353 The geometry is represented as a zero level-set of a neural 368
 354 network, similarly to the IGR approach. They also derived the 369
 355 rendering from the rendering equation, capable of (implicitly) 370
 356 modeling a broad set of lighting conditions and materials 371
 357 [16]. They trained the network on real-world 2D images of 372
 358 objects with different material properties, lighting conditions, 373
 359 and noisy camera initialization. Figure 12 presents an example 374
 360 of this technique.

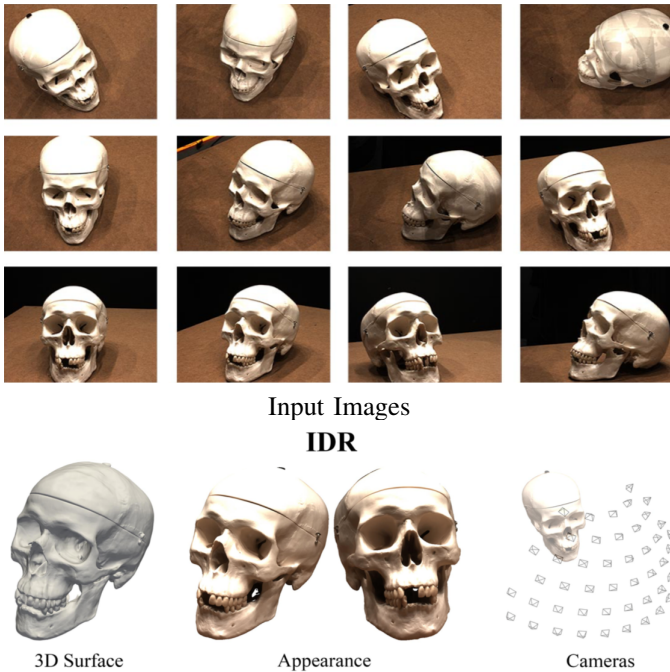


Fig. 12. An end-to-end learning of geometry, appearance and cameras from images.

VII. NETWORK OPTIMIZATION

361 Although the expressive results of neural networks in repre-
 362 senting 3D surfaces and implicit functions, we fall in performance
 363 problems when we consider real-time applications for
 364 these methods. In other words, it is unpractical to use these
 365

methods in real-time applications due to their computational 366
 complexity. In most cases, they fail when considering run- 367
 time performance or do not achieve the precision needed. We 368
 propose a strategy to improve performance of the SIREN based 369
 model considering a trade-off between runtime performance 370
 and accuracy. For each layer of SIREN, we use matrix 371
 factorizations to not only reduce dimensionality, but also to 372
 improve performance. We assume that each layer is over 373
 parameterized and its weights can be represented by a matrix 374
 or tensor with a lower rank. Actually, the idea of improving 375
 the performance of neural networks with matrix factorization 376
 is not new. The Faster-RCNN proposes the use of Singular 377
 Value Decomposition (SVD) for the fully connected layers. 378

A fully connected layer essentially does matrix multiplica- 379
 tion of its input x by a matrix A , and then adds a bias b : 380

$$Ax + b \quad (4)$$

We can decompose the matrix A , truncating it, keeping only 381
 the first r singular values as in Equation 5: 382

$$(U_{n \times r} S_{r \times r} V_{m \times r}^T)x + b = U_{n \times r}(S_{r \times r} V_{m \times r}^T x) + b \quad (5)$$

Instead of having one fully connected layer, now we have 2 383
 but with smaller weight matrices, where the first one is defined 384
 by $S_{r \times r} V_{m \times r}^T$ and the second by the matrix $U_{n \times r}$. The overall 385
 number of parameters drops from $n \times m$ to $r(n + m)$. 386

We know that estimating an optimal rank to approximate 387
 the original matrix can be sometimes difficult. We can try 388
 different values and check the accuracy, playing with heuristics 389
 that consider the trade-off between performance and accuracy. 390
 However, the rank selection should be automated. Considering 391
 this we can use a technique to estimate an optimal rank approx- 392
 imation for our layers considering the Variational Bayesian 393
 Matrix Factorization [21]. The VBMF is a probabilistic algo- 394
 rithm that approximates a matrix $V_{n \times m}$ as the sum of a 395
 lower ranking matrices $B_{n \times h} A_{h \times m}^T$ and gaussian noise. After 396
 A and B are found, h is an upper bound on the rank. The 397
 VB approximation has been successfully applied to matrix 398
 factorization, offering automatic dimensionality selection for 399
 principal component analysis [22]. Generally, finding the VB 400
 solution is a non-convex problem, and most methods rely on 401
 a local search algorithm derived through a standard procedure 402

403 for the VB approximation. Nakajima et.al [21]. presents a
 404 global analytical solution for the VBMF, where the global
 405 solution is a reweighted SVD of the observed matrix, and each
 406 weight can be obtained by solving a quartic equation with its
 407 coefficients being functions of the observed singular value.

408 We test this approach to automatically set an optimal rank
 409 to each layer of a Siren Neural Network. With this, we reduce
 410 the number of operations for this model by 10 times from
 411 the original. With this approach, it was possible to use the
 412 model in real-time applications, hlsl shader programs and RTX
 413 architecture. Figures 13 and 14 show different results of neural
 414 networks with 2 levels of decomposition.



Fig. 13. Result based on a decomposed SIREN with 1/8 of the original parameters size.



Fig. 14. Result based on a decomposed SIREN with 1/4 of the original parameters size.

VIII. CONCLUSION

415
 416 We have presented in this survey the state-of-the-art meth-
 417 ods for learning high-fidelity neural implicit representations of
 418 3D shapes. These methods can use different loss functions and
 419 activation functions. We described their different architectures
 420 and their limitations for real-time applications. At the end,
 421 we have proposed strategies to improve the performance and
 422 reduce computational complexity.

423 Due to Neural Implicit Representation's novelty, simplicity
 424 and impressive results, the possibilities for future works are
 425 fairly vast. There are numerous avenues for exploring its
 426 properties, such as sampling approaches to speed-up training
 427 convergence, using the approximate SDF values during train-
 428 ing to mitigate artifacts in the function domain.

429 More information about this research area can be found in
 430 the companion Web Portal of this survey: "Deep Implicits"
 431 (<https://lvelhoimpa.br/deep-implicits/>).

REFERENCES

- 432
 433 [1] A. Gropp, L. Yariv, N. Haim, M. Atzmon, and Y. Lipman, "Im-
 434 plicit geometric regularization for learning shapes," *arXiv preprint*
 435 *arXiv:2002.10099*, 2020.
 436 [2] T. Groueix, M. Fisher, V. G. Kim, B. C. Russell, and M. Aubry, "A
 437 papier-mâché approach to learning 3d surface generation," in *Proceed-*
 438 *ings of the IEEE conference on computer vision and pattern recognition*,
 439 2018, pp. 216–224.
 440 [3] T. Deprelle, T. Groueix, M. Fisher, V. G. Kim, B. C. Russell, and
 441 M. Aubry, "Learning elementary structures for 3d shape generation and
 442 matching," *arXiv preprint arXiv:1908.04725*, 2019.
 443 [4] F. Williams, T. Schneider, C. Silva, D. Zorin, J. Bruna, and D. Panozzo,
 444 "Deep geometric prior for surface reconstruction," in *Proceedings of the*
 445 *IEEE/CVF Conference on Computer Vision and Pattern Recognition*,
 446 2019, pp. 10 130–10 139.
 447 [5] A. Sinha, J. Bai, and K. Ramani, "Deep learning 3d shape surfaces
 448 using geometry images," in *European Conference on Computer Vision*.
 449 Springer, 2016, pp. 223–240.
 450 [6] A. Sinha, A. Unmesh, Q. Huang, and K. Ramani, "Surfnet: Generating
 451 3d shape surfaces using deep residual networks," in *Proceedings of the*
 452 *IEEE conference on computer vision and pattern recognition*, 2017, pp.
 453 6040–6049.
 454 [7] H. Maron, M. Galun, N. Aigerman, M. Trope, N. Dym, E. Yumer, V. G.
 455 Kim, and Y. Lipman, "Convolutional neural networks on surfaces via
 456 seamless toric covers." *ACM Trans. Graph.*, vol. 36, no. 4, pp. 71–1,
 457 2017.
 458 [8] L. M. Mescheder, M. Oechsle, M. Niemeyer, S. Nowozin, and
 459 A. Geiger, "Occupancy networks: Learning 3d reconstruction in
 460 function space." *CoRR*, vol. abs/1812.03828, 2018. [Online]. Available:
 461 <http://arxiv.org/abs/1812.03828>
 462 [9] Z. Chen and H. Zhang, "Learning implicit fields for generative shape
 463 modeling," 2019.
 464 [10] J. J. Park, P. Florence, J. Straub, R. Newcombe, and S. Lovegrove,
 465 "Deepsdf: Learning continuous signed distance functions for shape rep-
 466 resentation," in *Proceedings of the IEEE/CVF Conference on Computer*
 467 *Vision and Pattern Recognition*, 2019, pp. 165–174.
 468 [11] M. Michalkiewicz, "Implicit surface representations as layers in neural
 469 networks," in *International Conference on Computer Vision (ICCV)*.
 470 IEEE, 2019.
 471 [12] Z. Chen, A. Tagliasacchi, and H. Zhang, "Bsp-net: Generating compact
 472 meshes via binary space partitioning." *Proceedings of IEEE Conference*
 473 *on Computer Vision and Pattern Recognition (CVPR)*, 2020.
 474 [13] B. Deng, K. Genova, S. Yazdani, S. Bouaziz, G. Hinton, and
 475 A. Tagliasacchi, "Cvxnet: Learnable convex decomposition," June 2020.
 476 [14] S. Peng, M. Niemeyer, L. M. Mescheder, M. Pollefeys, and A. Geiger,
 477 "Convolutional occupancy networks," *CoRR*, vol. abs/2003.04618,
 478 2020. [Online]. Available: <https://arxiv.org/abs/2003.04618>
 479 [15] V. Sitzmann, J. Martel, A. Bergman, D. Lindell, and G. Wetzstein,
 480 "Implicit neural representations with periodic activation functions,"
 481 *Advances in Neural Information Processing Systems*, vol. 33, 2020.

- 482 [16] B. Mildenhall, P. P. Srinivasan, M. Tancik, J. T. Barron, R. Ramamoorthi,
483 and R. Ng, "Nerf: Representing scenes as neural radiance fields for view
484 synthesis," in *European conference on computer vision*. Springer, 2020,
485 pp. 405–421.
- 486 [17] L. Yariv, Y. Kasten, D. Moran, M. Galun, M. Atzmon, R. Basri, and
487 Y. Lipman, "Multiview neural surface reconstruction by disentangling
488 geometry and appearance," *arXiv preprint arXiv:2003.09852*, 2020.
- 489 [18] M. Atzmon, N. Haim, L. Yariv, O. Israelov, H. Maron, and Y. Lipman,
490 "Controlling neural level sets," *arXiv preprint arXiv:1905.11911*, 2019.
- 491 [19] M. Atzmon and Y. Lipman, "Sal: Sign agnostic learning of shapes from
492 raw data," in *Proceedings of the IEEE/CVF Conference on Computer
493 Vision and Pattern Recognition*, 2020, pp. 2565–2574.
- 494 [20] B. Curless and M. Levoy, "A volumetric method for building complex
495 models from range images," in *Proceedings of the 23rd annual confer-
496 ence on Computer graphics and interactive techniques*, 1996, pp. 303–
497 312.
- 498 [21] S. Nakajima, M. Sugiyama, S. D. Babacan, and R. Tomioka, "Global
499 analytic solution of fully-observed variational bayesian matrix factor-
500 ization," *Journal of Machine Learning Research*, vol. 14, no. Jan, pp.
501 1–37, 2013.
- 502 [22] S. Nakajima, R. Tomioka, M. Sugiyama, and S. D. Babacan, "Perfect
503 dimensionality recovery by variational bayesian pca." in *NIPS*, 2012, pp.
504 980–988.